

Progress on the $^{40}Ca^{+}$ ion optical clock

Baolin Zhang(张宝林), Yao Huang(黄垚), Huaqing Zhang(张华青), Yanmei Hao(郝艳梅), Mengyan Zeng(曾孟彦), Hua Guan(管桦), Kelin Gao(高克林)

Citation: Chin. Phys. B . 2020, 29(7): 074209 . **doi:** 10.1088/1674-1056/ab9432
Journal homepage: http://cpb.iphy.ac.cn; http://iopscience.iop.org/cpb

What follows is a list of articles you may be interested in

Improvement of 2.79-μm laser performance on laser diode side-pumped GYSGG/Er,Pr: GYSGG bonding rod with concave end-faces

Xu-Yao Zhao(赵绪尧), Dun-Lu Sun(孙敦陆), Jian-Qiao Luo(罗建乔), Hui-Li Zhang(张会丽), Zhong-Qing Fang(方忠庆), Cong Quan(权聪), Lun-Zhen Hu(胡伦珍), Zhi-Yuan Han(韩志远), Mao-Jie Cheng(程毛杰), Shao-Tang Yin(殷绍唐)

Chin. Phys. B . 2019, 28(11): 114208 . **doi:** 10.1088/1674-1056/ab4ce0

Non-crossover sub-Doppler DAVLL in selective reflection scheme

Lin-Jie Zhang(张临杰), Hao Zhang(张好), Yan-Ting Zhao(赵延霆), Lian-Tuan Xiao(肖连团), Suo-Tang Jia(贾锁堂)

Chin. Phys. B . 2019, 28(8): 084211 . **doi:** 10.1088/1674-1056/28/8/084211

Active hyperspectral imaging with a supercontinuum laser source in the dark

Zhongyuan Guo(郭中源), Yu Liu(刘煜), Xin Zheng(郑鑫), Ke Yin(殷科)

Chin. Phys. B . 2019, 28(3): 034206 . **doi:** 10.1088/1674-1056/28/3/034206

Nonlinear behavior of the population dynamics of three-level systems in the presence of single photon absorption

Allam Srinivasa Rao

Chin. Phys. B . 2019, 28(2): 024211 . **doi:** 10.1088/1674-1056/28/2/024211

Broad bandwidth interference filter-stabilized external cavity diode laser with narrow linewidth below 100 kHz

Guan-Zhong Pan(潘冠中), Bao-Lu Guan(关宝璐), Chen Xu(徐晨), Peng-Tao Li(李鹏涛), Jia-Wei Yang(杨嘉炜), Zhen-Yang Liu(刘振杨)

Chin. Phys. B . 2018, 27(1): 014204 . **doi:** 10.1088/1674-1056/27/1/014204

TOPICAL REVIEW — Ultracold atom and its application in precision measurement

Progress on the $^{40}Ca^{+}$ ion optical clock*

Baolin Zhang(张宝林)[1,2,3], Yao Huang(黄垚)[1,2], Huaqing Zhang(张华青)[1,2,3], Yanmei Hao(郝艳梅)[1,2,3], Mengyan Zeng(曾孟彦)[1,2,5], Hua Guan(管桦)[1,2,†], and Kelin Gao(高克林)[1,2,4,‡]

[1] *State Key Laboratory of Magnetic Resonance and Atomic and Molecular Physics, Wuhan Institute of Physics and Mathematics, Innovation Academy for Precision Measurement Science and Technology, Chinese Academy of Sciences (CAS), Wuhan* 430071, *China*

[2] *Key Laboratory of Atomic Frequency Standards, Wuhan Institute of Physics and Mathematics, Innovation Academy for Precision Measurement Science and Technology, Chinese Academy of Sciences, Wuhan* 430071, *China*

[3] *University of Chinese Academy of Sciences, Beijing* 100049, *China*

[4] *Center for Cold Atom Physics, Chinese Academy of Sciences, Wuhan* 430071, *China*

[5] *Huazhong University of Science and Technology, Wuhan* 430074, *China*

(Received 16 March 2020; revised manuscript received 18 May 2020; accepted manuscript online 19 May 2020)

Progress of the $^{40}Ca^{+}$ ion optical clock based on the $4^2S_{1/2}$–$3d\ ^2D_{5/2}$ electric quadrupole transition is reported. By setting the drive frequency to the "magic" frequency Ω_0, the frequency uncertainty caused by the scalar Stark shift and second-order Doppler shift induced by micromotion is reduced to the 10^{-19} level. By precisely measuring the differential static scalar polarizability $\Delta\alpha_0$, the uncertainty due to the blackbody radiation (BBR) shift (coefficient) is reduced to the 10^{-19} level. With the help of a second-order integrating servo algorithm, the uncertainty due to the servo error is reduced to the 10^{-18} level. The total fractional uncertainty of the $^{40}Ca^{+}$ ion optical clock is then improved to 2.2×10^{-17}, whereas this value is mainly restricted by the uncertainty of the BBR shift due to temperature fluctuations. The state preparation is introduced together with improvements in the pulse sequence, and furthermore, a better signal to noise ratio (SNR) and less dead time are achieved. The clock stability of a single clock is improved to $4.8\times10^{-15}/\sqrt{\tau}$ (in seconds).

Keywords: $^{40}Ca^{+}$ ion optical clocks, "magic" drive frequency, frequency uncertainty, frequency stability

PACS: 42.62.Fi, 37.10.Ty, 95.55.Sh, 06.20.–f **DOI:** 10.1088/1674-1056/ab9432

1. Introduction

Owing to their low uncertainty and instability, atomic optical frequency standards have found many irreplaceable and extremely important applications, such as in navigation and for tests of physical theories that need high precision. In the past two decades, the development of optical clocks has made great progress, surpassing the microwave Cs fountain clocks in terms of uncertainty and stability.

Optical frequency standards are mainly based on single ions trapped in ion traps such as Ba^{+}, Sr^{+}, Hg^{+}, In^{+}, Al^{+}, Yb^{+}, and Ca^{+},[1–5] or neutral atoms trapped in optical lattices such as Sr, Yb, and Hg.[6–10] Single-ion optical clocks always have simple ion-trap and optical systems as a single ion can be confined by a radio frequency (RF) potential for as long as several days or even a month. To date, the Al^{+} ion of NIST has achieved the smallest uncertainty of 9.4×10^{-19}.[11] Optical lattice clocks can provide better stability because of their large number of atoms. Benefiting from the development of the ultra-narrow-linewidth laser technology, the Sr lattice optical clock in JILA has achieved the best stability of $4.8\times10^{-17}/\sqrt{\tau}$ with the use of an ultra-stable clock laser based on cryogenic silicon reference cavities.[12] Another good stability of $1.5\times10^{-16}/\sqrt{\tau}$ has also been measured by NIST based on their Yb lattice optical clock.[8]

The optical clocks based on the $4^2S_{1/2}$–$3d\ ^2D_{5/2}$ electric quadrupole transition of a single trapped $^{40}Ca^{+}$ ion have been studied by our group at the Wuhan Institute of Physics and Mathematics (WIPM), Chinese Academy of Sciences in China for many years. The reason why we chose the $^{40}Ca^{+}$ ion is its relatively simple energy level structure and laser system in which all lasers mentioned in the energy-level scheme (Fig. 1) can be generated by diode lasers. However, compared with other ions, especially the Al^{+} ion, the $^{40}Ca^{+}$ ion has a greater blackbody radiation (BBR) shift and uncertainty.

For optical clocks, the most important criteria are low uncertainty and instability. In 2015, we achieved an uncertainty of 6.5×10^{-16} and a stability of $1.0\times10^{-14}/\sqrt{\tau}$ for a single $^{40}Ca^{+}$ optical clock.[13] To improve these two criteria, many efforts have been adopted. On one hand, we introduce the "magic" RF drive frequency to reduce the micromotion-

*Project supported by the National Key Research and Development Program of China (Grant Nos. 2017YFA0304401, 2018YFA0307500, 2017YFA0304404, and 2017YFF0212003), the National Natural Science Foundation of China (Grant Nos. 11622434, 11774388, 11634013, 11934014, and 91736310), the Strategic Priority Research Program of the Chinese Academy of Sciences (Grant No. XDB21030100), the CAS Youth Innovation Promotion Association (Grant Nos. Y201963 and 2018364), and the Science Fund for Distinguished Young Scholars of Hubei Province, China (Grant No. 2017CFA040).

†Corresponding author. E-mail: guanhua@wipm.ac.cn

‡Corresponding author. E-mail: klgao@wipm.ac.cn

© 2020 Chinese Physical Society and IOP Publishing Ltd

induced uncertainty,[3,14,15] a second-order integrating servo algorithm is applied to reduce the servo uncertainty,[14,16] and a $^{40}Ca^{+}$ optical clock cryogenic system cooled by liquid nitrogen is setting up to reduce the uncertainty of the BBR field evaluation of temperature.[15] On the other hand, we apply a state-preparation technology to increase the SNR of the clock transition, and the high-resolution timing control system based on the field-programmable gate arrays (FPGAs) and direct digital synthesizers (DDSs) to reduce dead time.[16] The SNR and dead time are crucial for the stability of optical clocks. Finally, we have obtained a total frequency uncertainty of 2.2×10^{-17} [15] and a stability of $4.8 \times 10^{-15}/\sqrt{\tau}$ based on an asynchronous comparison of two independent clocks. In this paper, we will go through each of these improvements in detail.

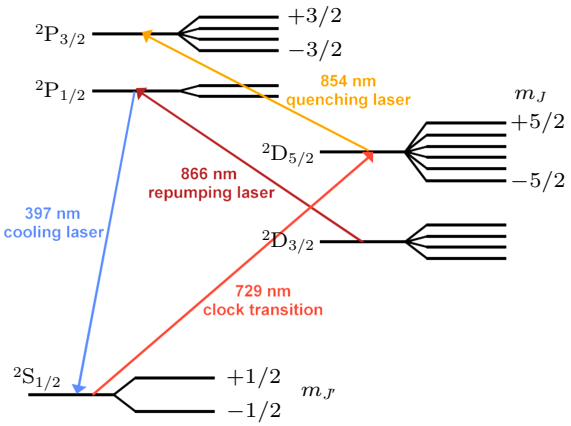


Fig. 1. Partial energy-level diagram of $^{40}Ca^{+}$ showing the transitions used in cooling, repumping, and probing.

2. Experimental setup

The $^{40}Ca^{+}$ ion optical clock system mainly consists of two parts. One is the ion trap system, containing an ion trap, a vacuum chamber, magnetic shields, and fluorescence detection devices. The other is a laser system, for the $^{40}Ca^{+}$ ion, which is composed of 397-nm, 866-nm, 854-nm, and 729-nm lasers and their frequency-stabilization devices.[17]

2.1. Ion trap system

In 2015, we used a miniature Paul ring trap to trap a $^{40}Ca^{+}$ ion. To reduce the shift and its uncertainty due to the secular motion, an ion trap with a lower heating rate is required. A new trap originally designed by NIST[11] with small modifications is adopted. A schematic diagram of this trap is shown in Fig. 2, and the vacuum chamber of the $^{40}Ca^{+}$ ion system is shown in Fig. 3. The outer vacuum chamber of the $^{40}Ca^{+}$ ion system is made of stainless steel. There are 6 glass windows on the periphery for laser access, and a glass window on the upper part for collection of the ion fluorescence. The clock transition can be split into 10 Zeeman components with a weak (in μT level) magnetic field.[18] Owing to the spinless nucleus of the $^{40}Ca^{+}$ ion, every component is very sensitive to the magnetic field. Small variations in the magnetic field could greatly broaden the spectrum of the clock transition; therefore, we installed two layers of magnetic shields outside the vacuum chamber to decrease this variation.

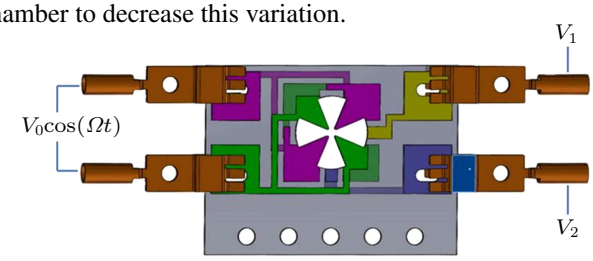


Fig. 2. Schematic diagram of the new linear Paul trap. $V_0\cos(\Omega t)$ is the RF potential. V_1 and V_2 are the horizontal and vertical compensation voltages, which are used to compensate for the static electric stray field at the center of the ion trap.



Fig. 3. Vacuum chamber and fluorescence collection devices of a $^{40}Ca^{+}$ ion optical clock.

2.2. Laser system

As shown in Fig. 1, the $^{40}Ca^{+}$ ion has a simple energy level system. Only 4 lasers with wavelengths of 397 nm, 866 nm, 854 nm, and 729 nm are used. The strongly allowed $4^2S_{1/2} \rightarrow 4^2P_{1/2}$ dipole transition is used for cooling, with a corresponding wavelength of 397 nm. For the cooling process, it is necessary to use an 866-nm laser to repump the ion from the metastable state $3^2D_{3/2}$ return to the S–P cooling branch, as there is a chance that the ion decays from the $4^2P_{1/2}$ state to the $3^2D_{3/2}$ state. After being excited to the $3^2D_{5/2}$ state by a probe pulse, the state of the ion will be read out by fluorescence detection. Another 854-nm laser is used to clear out the $3^2D_{5/2}$ metastable state after each interrogation. In the laser system, the 397-nm and 866-nm lasers are generated by commercial diode lasers and stabilized by an ultra-low expansion (ULE) cavity. The ultra-stable clock laser is stabilized by a 10-cm-long ULE reference cavity with a stability of $\sim 1 \times 10^{-15}$ at 1 s–20 s. Because a high pumping efficiency can be obtained within a large frequency range for the 854-nm laser, there is no frequency-stabilization device for it. The frequencies and amplitudes of all lasers are manipulated by acousto-optic modulators (AOMs). We only need to change the RFs generated

by the DDSs to change the frequencies and amplitudes of the laser beams or switch it on and off.

3. Time sequence control system

In this work, the improvements on the pulse sequence mainly focus on a reduction in dead time and the introduction of state-preparation technology. The new control system based on the FPGAs and DDSs can alter the RFs applied to the AOMs within a few microseconds. Then, we can change the frequency and power of the cooling laser beam many times within one cycle to realize optimal cooling and fluorescence-detection efficiency simultaneously. The dead time caused by modifying all RFs is negligible. Moreover, with the implementation of the state preparation nearly double the previous excitation probability on the resonance of the clock transition can be achieved, which means a lower instability.

3.1. Cooling and detection pulses

Figure 4 shows the spectrum of the transition of $4^2S_{1/2} \longrightarrow 4^2P_{1/2}$ used for cooling and fluorescence detection in $^{40}Ca^+$ ion optical clocks. Three detuning frequencies (precooling, Doppler-cooling, and PMT shown in Fig. 4) are used for cooling and detection. First, the cooling laser is far-red detuned (precooling point), then near-red detuned (Doppler-cooling point) by approximately half the linewidth from the cooling transition line center to further cool the ion. In the cooling stage, the 866-nm laser beam is switched on to repump the ion to the $4^2P_{1/2}$ state, due to the branching fraction of the decay of the $4^2P_{1/2}$ state to the $4^2S_{1/2}$ state. One reason for dividing the cooling process into two stages is that the 854-nm-laser pulse is inevitably required to clear out the $^2D_{5/2}$ state after each interrogation, so the first cooling process can be merged into it. The other is that if the ion is very hot, Doppler cooling will be less efficient than precooling. The measured temperature of the cooled ion is 1.0(5) mK, which is close to the Doppler cooling limit.[18]

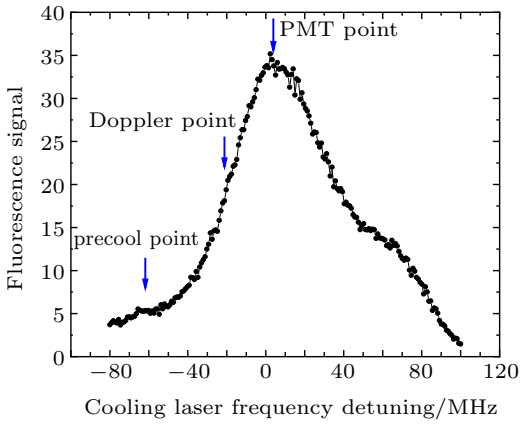


Fig. 4. Spectrum of the cooling transition of $^{40}Ca^+$ ion. There are three frequency detuning points, which are used in precooling, Doppler cooling, and PMT detection. The goal is to achieve optimal efficiency for each process.

As shown in Fig. 4, the strongest fluorescence signal can be obtained at the PMT point.[13] The FPGAs and DDSs control systems can implement the cooling and detection pulses at different frequencies without introducing additional dead time. The final state of the $^{40}Ca^+$ ion after interrogation can be distinguished by a state detection pulse. If the $^{40}Ca^+$ ion is in metastable state $^2D_{5/2}$, only the background fluorescence signal can be obtained. By optimizing the imaging mirror and the related parameters of the 397-nm and 866-nm lasers, we obtained an average fluorescence count of 30 in a 0.5-ms-long detection, with a background count of less than 6.

3.2. State preparation

For the $^{40}Ca^+$ ion, the ground state $^2S_{1/2}$ has two magnetic sublevels with equal probability, so the greatest excited probability for each Zeeman component is only ~ 0.5, as there is only a 50% chance that the ion is in the $^2S_{1/2}(m = +1/2)$ or $^2S_{1/2}(m = -1/2)$ states initially. Initial state preparation can increase the transition probability twice and improve the stability by $\sim \sqrt{2}$ times.[16,19] Many methods can be used to implement state preparation, depending on the energy-level structure of the ion and the requirements of the experiment.[19] In our lab, we chose the frequency-resolved optical pumping on the clock transition. Compared with the optical pumping of circularly polarized light on the cooling transition, it takes more time but only requires a simple setup.[20] Specifically, as shown in Fig. 5, the probe laser's frequency is set at the resonance of one of the two transitions of $^2S_{1/2}(m = +1/2) \rightarrow {}^2D_{5/2}(m = +1/2)$ or $^2S_{1/2}(m = -1/2) \rightarrow {}^2D_{5/2}(m = -1/2)$ state to pump the ion from the $^2S_{1/2}$ to the $^2D_{5/2}$ state. An 854-nm-laser pulse will pump the ion from the $^2D_{5/2}$ state to the $^2P_{3/2}$ state and then it will decay to the two $^2S_{1/2}(m = \pm 1/2)$ states with equal probability.

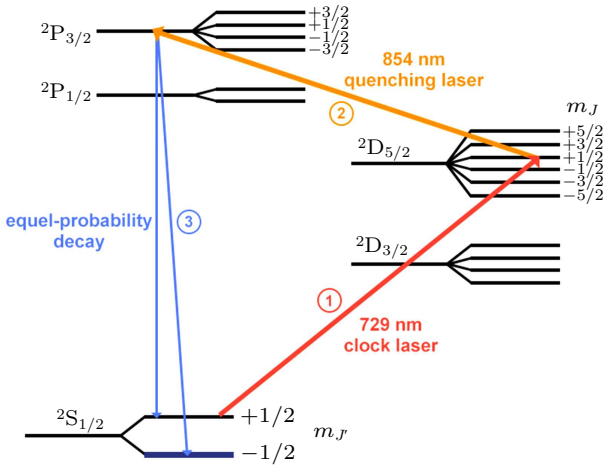


Fig. 5. Schematic diagram of the state preparation. Firstly the $^{40}Ca^+$ ion is excited to the metastable $^2D_{5/2}(m = +1/2)$ state form the $^2S_{1/2}(m = +1/2)$ state by the 729-nm laser, then to the $^2P_{3/2}$ state by the 854-nm laser, and spontaneously decay to the two grounds with equal probability from the $^2P_{3/2}$ state. After several times, the $^{40}Ca^+$ ion would be pumped to the $^2S_{1/2}(m = -1/2)$ state.

By repeating this cycle for approximately 5 times, we obtained $a > 95\%$ probability of preparing the $^{40}Ca^{+}$ ion in one of the two ground states. Figure 6 shows the Zeeman-resolved spectrum with and without state preparation.

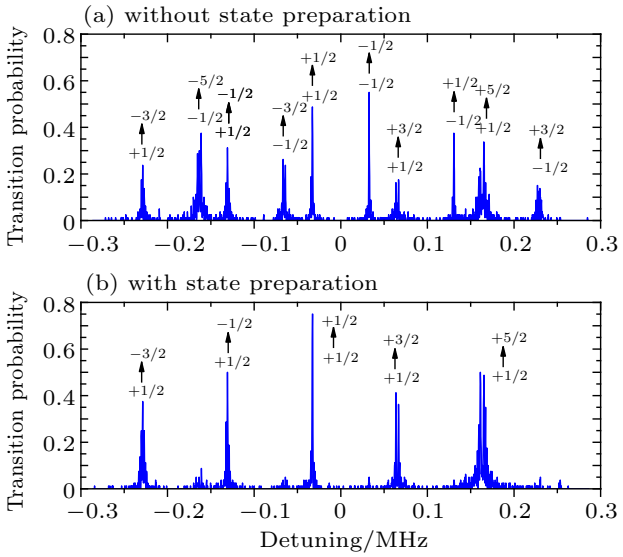


Fig. 6. Zeeman-resolved spectra of the $^2S_{1/2} \rightarrow {}^2D_{5/2}$ transition of a single $^{40}Ca^{+}$ ion obtained at the same probe laser power. The ground state sublevel $m_J = \pm 1/2$ and the upper state sublevel $m_{J'}$ ($^2D_{5/2}$) are shown below and above each arrow respectively. (a) Spectrum shows 10 Zeeman components completely and is obtained without state preparation. In the (b) spectrum, the $^{40}Ca^{+}$ ion has been pumped to the $^2S_{1/2}(m = +1/2)$ state; thus, only 5 Zeeman components are obtained, but with a higher transition probability.

3.3. Probing pulse

In the interrogation, other lasers, except for the probe laser, have been switched off by mechanical shutters instead of the AOMs to cancel other lasers' AC Stark shift.[14,21] It adds a 5-ms-long dead time twice, for opening or closing the mechanical shutter before or after the integration, respectively. In this experiment, the two clocks share the same clock laser and timing control system, *i.e.*, for the two clocks, the interrogation is asynchronous. To improve the stability compared to the previous result,[13] we choose the Ramsey scheme with which a single π-pulse is separated equally by a free evolution time T_{free}. For a sufficiently short pulse duration, the linewidth of the central fringe is independent of the Rabi pulsation and is equal to $1/2T_{\text{free}}$.[16] This is much narrower than the Rabi result on the condition of the same time spent in the interrogation.

3.4. Clock transition spectroscopy

For a single ion system, to obtain the transition probability at each frequency point, the ion needs to be interrogated multiple times with the same parameters, and the successful excitations will be counted. For the $^2S_{1/2} \rightarrow {}^2D_{5/2}$ transition, if the ion is found in the $^2D_{5/2}$ state by detection after interrogation, it has been excited successfully.[22] Thirty integrations at each frequency point were taken, and a Ramsey spectrum with a free evolution time of 80 ms is obtained, as shown in Fig. 7. More integrations can reduce the uncertainty of the transition probability, but take longer time.

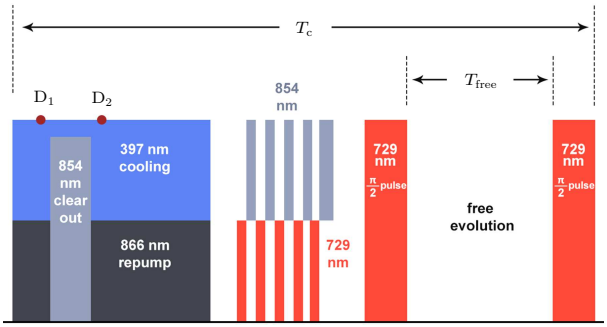


Fig. 7. The pulse sequence for one interrogation cycle. In this experiment, the free evolution time is $T_{\text{free}} = 80$ ms and the time for one cycle is $T_c = 99.6$ ms. The fluorescence is collected at D_1 for state detection and at D_2 to verify that the ion has returned to the S state after an 854-nm pulse.

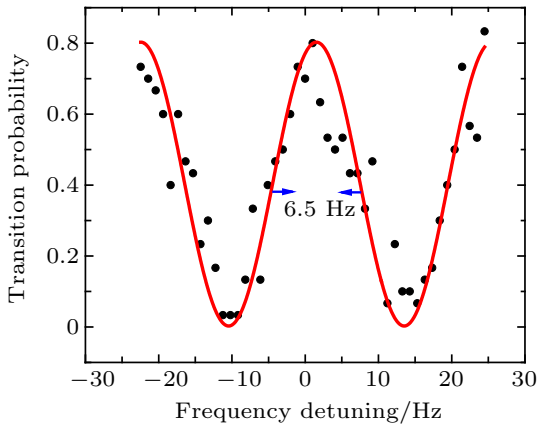


Fig. 8. The high-resolution spectrum with a free evolution time of 80 ms. The black points are the probabilities of the clock transition and the red solid line is the fitting result of a Ramsey line shape, corresponding to a linewidth of approximately 6.5 Hz.

4. Evaluation of systematic frequency shifts

A variety of potential sources might be associated with the $^2S_{1/2} \rightarrow {}^2D_{5/2}$ electric-quadrupole transition of a laser-cooled trapped $^{40}Ca^{+}$ ion, causing a frequency shift and uncertainty. They have been evaluated in our previous work.[14,21] In this paper, we report the recent progress on the evaluation of the scalar Stark shift and the second-order Doppler shift induced by excess micromotion, the BBR shift, and the servo shift.

4.1. Excess micromotion uncertainty induced by scalar Stark shift and second-order Doppler shift

Figure 2 shows a schematic diagram of the latest ion trap, modified by a linear Paul trap. The potential near the axis of the trap can be approximated by[23]

$$U(x,y,z) = \frac{V_0}{2}\left(1 + \frac{x^2 - y^2}{R^2}\right)\cos(\Omega t)$$

$$+\frac{\kappa U_0}{Z_0^2}\left[z^2-\frac{1}{2}(x^2+y^2)\right], \tag{1}$$

where $V_0\cos(\Omega t)$ and U_0 are the potential added to the electrodes and endcaps, respectively, R is the perpendicular distance from the trap axis to the trap electrodes, $\kappa(<1)$ is a geometrical factor, and Z_0 is the distance between the two cap electrodes. After solving the Mathieu equation, we obtain the position of the ion in a typical case with $|q_i| \ll 1$ and $|a_i| \ll 1$[23]

$$a_x = a_y = -\frac{1}{2}a_z = -\frac{4e\kappa U_0}{mZ_0^2\Omega^2}, \tag{2}$$

$$q_x = -q_y = \frac{2eV_0}{mR'^2\Omega^2}, \quad q_z = 0, \tag{3}$$

$$u_i(t) \approx u_{1i}\cos(\omega_i t+\varphi_{\rm Si})\left[1+\frac{q_i}{2}\cos(\Omega t)\right], \tag{4}$$

where u_i is the position of the ion $(i=x,y,z)$, $\varphi_{\rm Si}$ is the initial phase, and $\omega_i \approx \frac{1}{2}\Omega\sqrt{a_i+\frac{1}{2}q_i^2}$ is the secular motion angular frequency. u_{1i} is the amplitude of the secular motion, reflecting the ion temperature, which can be reduced by Doppler or sideband cooling.

If we consider a uniform static electric field $\boldsymbol{E}_{\rm dc}$, equation (4) becomes[23]

$$u_i(t) \approx [u_{0i}+u_{1i}\cos(\omega_i t+\varphi_{\rm Si})] \times\left[1+\frac{q_i}{2}\cos(\Omega t)\right], \tag{5}$$

where

$$u_{0i} = \frac{4eE_i}{m(a_i+\frac{1}{2}q_i^2)\Omega^2}. \tag{6}$$

The field $\boldsymbol{E}_{\rm dc}$ displaces the averaging position u_{0i} $(i=x,y,z)$ from the center of the trap, and induces a micromotion with an amplitude of $\frac{1}{2}u_{0i}q_i$ and an angular frequency Ω. This excess micromotion is caused by a uniform static electric field $\boldsymbol{E}_{\rm dc}$ and the AC electric fields of the trap. From the expression of its amplitude, one can ascertain that it cannot be reduced by cooling, but it can be evaluated by monitoring the change of the ion's place with a high-resolution camera, while the trap depth is alternated between strong and weak. Moreover, by varying the trim electrode voltages, we can find a set of ideal parameters where the position of the ion does not change with the trap depth. This was the most effective way to minimize excess micromotion in our previous work.[14,21]

Ion movement can create a second-order Doppler (time-dilation) shift and a scalar AC Stark shift due to the AC field the ion experiences. If we consider only the shifts caused by the excess micromotion, they are approximately[3,15,23]

$$\frac{\Delta\nu_\mu}{\nu_0} = -\frac{1}{2}\frac{\langle V\rangle^2}{c^2}-\frac{\Delta\alpha_0}{2h}\langle E^2\rangle, \tag{7}$$

where $\Delta\alpha_0 = \alpha_0\left(\mathrm{D}_{5/2}\right)-\alpha_0\left(\mathrm{S}_{1/2}\right)$ is the differential static scalar polarizability of the clock transition.

From Eqs. (1) and (5), we can obtain the AC electric field and the velocity of the ion. By placing the position obtained in Eq. (5) to the AC electric field, equation (7) can be simplified to[3,15,23]

$$\frac{\Delta\nu_\mu}{\nu_0} = -\left(\frac{\Omega}{\omega_0}\right)^2\left[1+\frac{\Delta\alpha_0}{\hbar\omega_0}\left(\frac{m\Omega c}{e}\right)^2\right]\sum_{x,y,z}R_i, \tag{8}$$

where R_i is the micromotion sideband-to-carrier intensity ratio of one Zeeman component. For the $^{40}Ca^+$ ion, $\Delta\alpha_0$ is a negative value, so we can choose a drive frequency of $\Omega_0 \approx (e/mc)\sqrt{-h\nu_0/\Delta\alpha_0}$ to cancel the scalar Stark shift and second-order Doppler shift induced by excess micromotion. The frequency Ω_0 is called the "magic" trap drive frequency.

The experiment of measuring the frequency Ω_0 is based on the comparison of two clocks (clock 1 and clock 2). Clock 1 is used to provide a constant standard frequency reference, and clock 2 is a test trap to study the change in micromotion shifts with trap drive frequency Ω. To begin with, all indicators of frequency shift and uncertainty of both clocks were optimized to the best with a fractional frequency uncertainty of $\sim 3\times10^{-17}$. We can guarantee that the transition frequency of clock 1 is a constant value within the uncertainty level, and that any frequency change exceeding the uncertainty level of clock 2 is entirely caused by micromotion. The DC offset voltage of clock 2 is trimmed to induce a relatively large micromotion level in the ion for an obvious comparison. Then, the frequency difference of the two clocks is due to the micromotion shift of clock 2. The drive frequency of clock 2 is tuned from 22 MHz to 27 MHz and the frequency difference at each point was measured, as shown in Fig. 9.[15]

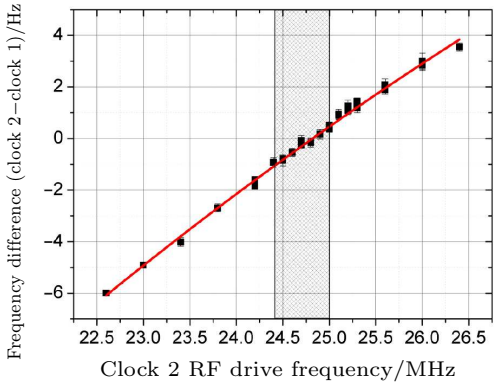


Fig. 9. Frequency difference between the two $^{40}Ca^+$ ion clocks as a function of the RF drive frequency of clock 2. The red curve is a fit to the data and gives $\Omega_0 = 2\pi\times24.81(1)$ MHz. The shaded area illustrates the uncertainty in the theoretical result.[15]

To obtain the value of $\Delta\alpha_0$ with a lower uncertainty by Ω_0, we have to consider the micromotion at the trap drive harmonics $n\Omega$. The total scalar Stark shift and the time-dilation

shift can be expressed as[3,15]

$$\Delta\nu_\mu = -\frac{\nu_0}{2}\sum_i\sum_{n=1}^{\infty}\left[\frac{\Delta\alpha_0}{h\nu_0}+\frac{1}{n^2}\left(\frac{e}{m\Omega c}\right)^2\right]\left\langle E_i^2(n\Omega)\right\rangle. \quad (9)$$

By solving Eq. (9), $\Delta\alpha_0$ is calculated to be $-7.2677(21)\times10^{-40}$ J·m^2·V^{-2}.[15] From Eq. (8) and the previous evaluation method, we evaluated an excess micromotion fractional uncertainty of 4×10^{-19}.[15]

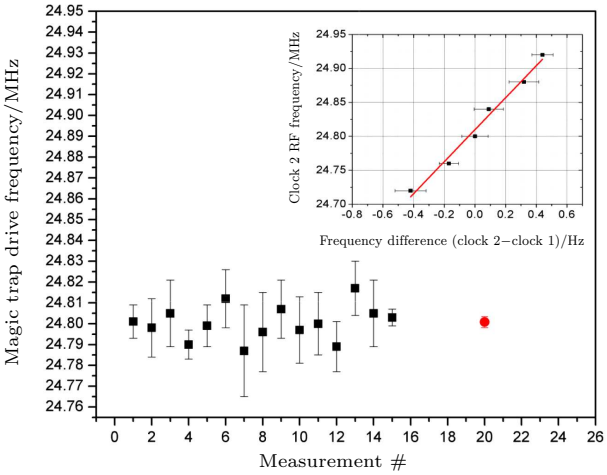


Fig. 10. Measurement of Ω_0 obtained by scanning the RF drive frequency of clock 2. To reduce the measurement statistical uncertainty of Ω_0, we repeated this scanning randomly from 24.7 MHz to 24.95 MHz 15 times. Fifteen scans were recorded (data shown as black squares). The corresponding weighted mean of Ω_0 is shown by the red circle. The inset shows the data taken in one of the scans and a linear fit through the data as shown in Fig. 8. and obtained the result of $\Omega_0 = 2\pi\times24.801(2)$ MHz.[15]

4.2. Blackbody radiation (BBR) shift of coefficient $\Delta\alpha_0$

To date, the BBR shift uncertainty is the main source of the total uncertainty for the $^{40}Ca^+$ ion.[24] The BBR shift of the S–D transition can be expressed as[25–27]

$$\Delta\nu_{\rm BBR} = -\frac{1}{2h}\left(\frac{831.943\ {\rm V}}{m}\right)^2\left(\frac{T}{300\ {\rm K}}\right)^4 \times\Delta\alpha_0(1+\eta), \quad (10)$$

where T is the BBR field temperature, h is Planck's constant, and η is a temperature-dependent dynamic correction to $\Delta\alpha_0$. From Eq. (10), the BBR shift uncertainty is caused by two parts: the uncertainty of coefficient $\Delta\alpha_0$ and temperature T. By using the value of $-7.2677(21)\times10^{-40}$ J·m^2·V^{-2}, the uncertainty caused by the BBR shift (coefficient $\Delta\alpha_0$) at room temperature has been reduced to 3×10^{-19},[15] benefiting from the calculated coefficient $\Delta\alpha_0$ having a lower uncertainty than the theoretical value.

4.3. Servo

In contrast to optical lattice atomic clocks, a single interrogation of a single ion can only provide one binary unit of information. In one frequency feedback cycle, the ion should be interrogated multiple times on the two sides of each Zeeman component to obtain the transition probabilities or error signal. The probe laser's frequency is f and the ion is interrogated n times at the frequencies of $f_+ = f+\delta_m/2$ and $f_- = f-\delta_m/2$ respectively, where δ_m is the linewidth. After counting the successful excitations n_+ at f_+ and n_- at f_-, the error signal and the frequency modification of the probe laser can be expressed as follows:[16,22]

$$e = \delta_m\frac{n_+-n_-}{n_++n_-}, \quad (11)$$

$$f \leftarrow f+g\cdot e, \quad (12)$$

where g is a numerical coefficient, called "gain". A frequency correction $g\cdot e$ is added to the laser frequency by an AOM to compensate for any frequency change of the clock laser stabilized by an ULE reference cavity. The servo algorithm is used to lock the frequency of the probe laser to the resonance of the clock transition. In this section, the clock laser refers to the laser beam stabilized by the reference cavity, and the probe laser represents the beam that passes through the position of the ion after modulated by an AOM.

Generally, the frequency of the clock laser is subject to drift with a nonlinear rate, similar to the probe laser between each frequency modification. However, for an ion optical clock, each feedback takes about a few seconds or more. The probe laser's frequency may change significantly and randomly owing to the noise of the reference cavity. This will cause a significant servo shift and error. A second-order integrating servo algorithm is introduced to obtain the current drift rate by the analysis of the latest frequencies, which reduces the servo error[14,16,28]

$$e_{\rm dr} = \text{linear fitting}[f_1,\ldots,f_N], \quad (13)$$

where $e_{\rm dr}$ refers to the current drift rate, $[f_1,\ldots,f_N]$ are the latest N frequencies, and N is determined by the drift characteristics of the clock laser. Then, the modified frequency of the probe laser in the next servo cycle can be expressed as[16]

$$f \rightarrow f+g\cdot e+g_1\cdot e_{\rm dr}, \quad (14)$$

where g_1 is another numerical coefficient.

Benefiting from the implementation of a second-order integrating servo algorithm and a longer probe time, the servo-error uncertainty is reduced to 7.6×10^{-18}.[15]

4.4. $^{40}Ca^+$ uncertainty budget

Table 1 summarizes the latest results of the systematic shifts and their uncertainties for the $^{40}Ca^+$ ion in our group. The total fractional uncertainty obtained by adding the contributions in quadrature is 2.2×10^{-17}. The BBR shift (temperature) is the largest contribution to the total uncertainty, but it can be reduced by lowering the temperature of the ion surroundings or a more accurate evaluation of the temperature.

Table 1. System shifts and uncertainties for the evaluation of the $^{40}Ca^{+}$ ion.[15]

Effect	Shift/10^{-18}	Uncertainty/10^{-18}
BBR field evaluation (temperature)	863	19
BBR coefficient $\Delta\alpha_0$ including dynamic correction	0	0.3
Excess micromotion	0	0.4
Second-order Doppler (thermal motion)	–11.4	5.5
AC Stark shift	1.2	1.3
Residual quadrupole	0	3.6
Zeeman effect	0	1.5
Servo	2.2	7.6
Total	885	22

5. Stability of $^{40}Ca^{+}$ ion optical clock

Stability is an important criterion for optical clocks besides uncertainty. To measure the frequency stability of a $^{40}Ca^{+}$ ion optical clock, we compared the frequency difference between two independent clocks continuously for approximately 38 h. In this experiment, both clocks have independent physical and optical systems, except for the probe laser, which is stabilized by a 10-cm-long ULE cavity.[17] Both $^{40}Ca^{+}$ ions are interrogated asynchronously. To cancel the electric quadrupole shift and quadratic Stark shift, we lock the probe laser to two pairs of the Zeeman components.[14,29] One pair is $^2S_{1/2}(m=+1/2) \rightarrow {}^2D_{5/2}(m=+1/2)$ and $^2S_{1/2}(m=-1/2) \rightarrow {}^2D_{5/2}(m=-1/2)$, and the other is $^2S_{1/2}(m=-1/2) \rightarrow {}^2D_{5/2}(m=-3/2)$ and $^2S_{1/2}(m=+1/2) \rightarrow {}^2D_{5/2}(m=+3/2)$. The pulse sequence is shown in Fig. 7. Eight frequency points on the left and right sides of the 4 Zeeman components are interrogated. To obtain the excited probability on each point or the total error signal, the same interrogation at each point is repeated 10 times.

The center frequency of the $^2S_{1/2} \rightarrow {}^2D_{5/2}$ transition for the $^{40}Ca+$ ion can be computed by the frequencies of the four Zeeman components[14,30]

$$f_{\text{center}} = \frac{4}{3} \cdot \frac{f_1 + f_2}{2} - \frac{1}{3} \cdot \frac{f_3 + f_4}{2}, \tag{15}$$

where f_1 and f_2 are the frequencies of the transitions of $^2S_{1/2}(m=\pm1/2) \rightarrow {}^2D_{5/2}(m=\pm1/2)$, and f_3 and f_4 are the frequencies of the transitions of $^2S_{1/2}(m=\pm1/2) \rightarrow {}^2D_{5/2}(m=\pm3/2)$. The frequency difference of the two clocks is obtained from the RF frequencies applied to the AOMs as they share the same clock laser. Figure 11 shows the results of the frequency difference of each comparison. The stability of each Ca^{+} optical clock is $4.8 \times 10^{-15}/\sqrt{\tau}$, which is deduced from the Allan deviation of the comparison between the two clocks, as shown in Fig. 12.

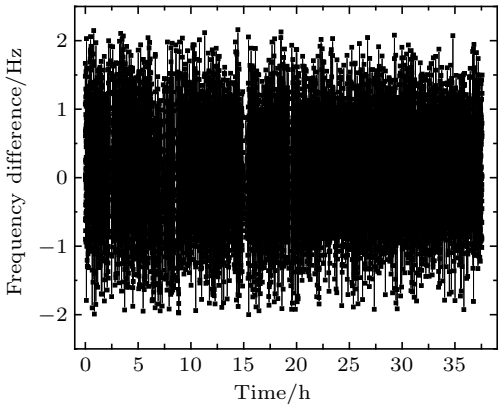


Fig. 11. Frequency difference between two $^{40}Ca^{+}$ ion optical clocks.

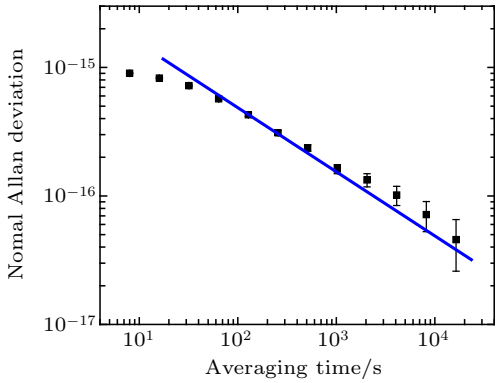


Fig. 12. Normal Allan deviation is measured for a single clock. The stability of a single clock is achieved by dividing $\sqrt{2}$ the Allan deviation of the comparison of two clocks. The result is $4.8 \times 10^{-15}/\sqrt{\tau}$.

6. Summary and prospects

To improve the performance of the $^{40}Ca^{+}$ optical clock, several efforts have been made in recent years. For the uncertainty, we precisely measured the "magic" trap drive frequency Ω_0 at which the shift of the scalar Stark and second-order Doppler induced by excess micromotion can cancel each other, corresponding to an uncertainty of below 1×10^{-18}. Then, the differential static scalar polarizability $\Delta\alpha_0$ is obtained by using the measured "magic" trap drive frequency Ω_0, with an uncertainty about 40 times smaller than the value of the theoretical calculation. Benefiting from the more accurate value of $\Delta\alpha_0$, the uncertainty due to the BBR shift (coefficient) has also been evaluated to be 3×10^{-19}. Additionally, the servo error uncertainty is also reduced to the 10^{-18} level by introducing a second-order integrating servo algorithm. Finally, the total uncertainty of the $^{40}Ca^{+}$ ion optical clock is evaluated to be 2.2×10^{-17}. For stability, we increased the pulse length to 80 ms and obtained a high-resolution Ramsey spectrum with a linewidth of approximately 6.5 Hz. The time spent on cooling and detection has been reduced significantly by changing the frequency of the cooling laser on the precooling, Doppler, and detection pulses. Furthermore, by preparing $^{40}Ca^{+}$ ion in one of the two ground states, the transition probability is double than before, which greatly reduces the QPN.

With these improvements, the Allan deviation is measured to be $4.8 \times 10^{-15}/\sqrt{\tau}$ by a Ramsey-excited comparison of two independent $^{40}Ca^{+}$ ion optical clocks.

For the BBR shift due to temperature fluctuations, according to Eq. (10), the frequency shift is related to T^4. Then, lowering the temperature around the ion can significantly reduce the BBR shift (temperature) as well as its uncertainty. In our laboratory environment, the temperature is measured as 21.0(1.5) °C (294.15(1.5) K), corresponding to a 7.8-mHz frequency uncertainty.[18] It is difficult to evaluate the room temperature with a lower uncertainty under existing experimental conditions. Therefore, we are setting up a liquid nitrogen cryogenic system as shown in Fig. 13, which puts the ion at the temperature of liquid nitrogen of approximately −196 °C (77.15 K). The shift at liquid nitrogen temperature can be reduced by two orders of magnitude smaller to the uncertainty under the same temperature uncertainty assessment. The new system is expected to be able to evaluate the uncertainty of the BBR shift (temperature) to the 10^{-18} level.

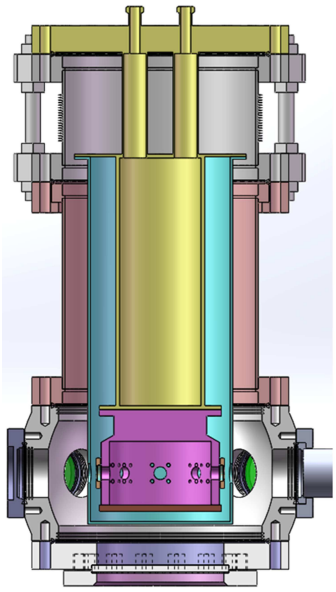


Fig. 13. The liquid nitrogen cryogenic $^{40}Ca^{+}$ ion optical clock system.

The stability of the $^{40}Ca^{+}$ ion optical clocks is ultimately limited by its metastable state lifetime of 1.16 s.[31] For Rabi interrogation, this limit is $\sigma_y(\tau) \approx 9.3 \times 10^{-16}/\sqrt{\tau}$ for a probe time of ≈ 1.5 s. For Ramsey interrogation, this limit is $\sigma_y(\tau) \approx 6.2 \times 10^{-16}/\sqrt{\tau}$ for a free evolution time of ≈ 1 s.[16,19]

Lower instability for single-ion optical clocks can be obtained by a longer probe time, which will be adopted in the future, with the help of a lower frequency noise by the clock laser and a shorter dead time.

Acknowledgments

The authors would like to thank Tingyun Shi, Zongchao Yan, Chengbin Li, Liyan Tang, Pierre Dube, and David Leibrandt for their cooperation and fruitful discussions.

References

[1] Barwood G P, Huang G, Klein H A, Johnson L A M, King S A, Margolis H S, Szymaniec K and Gill P 2014 *Phys. Rev. A* **89** 050501
[2] Chou C W, Hume D B, Koelemeij J C J, Wineland D J and Rosenband T 2010 *Phys. Rev. Lett.* **104** 070802
[3] Dubé P, Madej A A, Tibbo M and Bernard J E 2014 *Phys. Rev. Lett.* **112** 173002
[4] Huntemann N, Sanner C, Lipphardt B, Tamm C and Peik E 2016 *Phys. Rev. Lett.* **116** 063001
[5] Rosenband T, Hume D B, Schmidt P O, Chou C W, Brusch A, Lorini L, Oskay W H, Drullinger R E, Fortier T M, Stalnaker J E, Diddams S A, Swann W C, Newbury N R, Itano W M, Wineland D J and Bergquist J C 2008 *Science* **319** 1808
[6] Campbell S L, Hutson R B, Marti G E, Goban A, Darkwah Oppong N, McNally R L, Sonderhouse L, Robinson J M, Zhang W, Bloom B J and Ye J 2017 *Science* **358** 90
[7] Campbell S L, Hutson R B, Marti G E, Goban A, Darkwah Oppong N, McNally R L, Sonderhouse L, Robinson J M, Zhang W, Bloom B J and Ye J 2017 *Science* **358** 90
[8] McGrew W F, Zhang X, Fasano R J, Schäffer S A, Beloy K, Nicolodi D, Brown R C, Hinkley N, Milani G, Schioppo M, Yoon T H and Ludlow A D 2018 *Nature* **564** 87
[9] Nicholson T L, Campbell S L, Hutson R B, Marti G E, Bloom B J, McNally R L, Zhang W, Barrett M D, Safronova M S, Strouse G F, Tew W L and Ye J 2015 *Nat. Commun.* **6** 6896
[10] Ushijima I, Takamoto M, Das M, Ohkubo T and Katori H 2015 *Nat. Photon.* **9** 185
[11] Brewer S M, Chen J S, Hankin A M, Clements E R, Chou C W, Wineland D J, Hume D B and Leibrandt D R 2019 *Phys. Rev. Lett.* **123** 033201
[12] Oelker E, Hutson R B, Kennedy C J, Sonderhouse L, Bothwell T, Goban A, Kedar D, Sanner C, Robinson J M, Marti G E, Matei D G, Legero T, Giunta M, Holzwarth R, Riehle F, Sterr U and Ye J 2019 *Nat. Photon.* **13** 714
[13] Guan H, Huang Y, Liu P L , Bian W, Shao H and Gao K L 2015 *Chin. Phys. B* **24** 054213
[14] Dubé P, Madej A A, Zhou Z and Bernard J E 2013 *Phys. Rev. A* **87** 023806
[15] Huang Y, Guan H, Zeng M, Tang L and Gao K 2019 *Phys. Rev. A* **99** 011401
[16] Peik E, Schneider T and Tamm C 2006 *J. Phys. B: At. Mol. Opt. Phys.* **39** 145
[17] Bian W, Huang Y, Guan H, Liu P, Ma L and Gao K 2016 *Rev. Sci. Instrum.* **87** 063121
[18] Huang Y, Guan H, Bian W, Ma L, Liang K, Li T and Gao K 2017 *Appl. Phys. B* **123** 166
[19] Dubé P, Madej A A, Shiner A and Jian B 2015 *Phys. Rev. A* **92** 042119
[20] Zeng M Y , Huang Y, Shao H, Wang M, Zhang H Q , Zhang B L , Guan H and Gao K L 2018 *Chin. Phys. Lett.* **35** 074202
[21] Huang Y, Guan H, Liu P, Bian W, Ma L, Liang K, Li T and Gao K 2016 *Phys. Rev. Lett.* **116** 013001
[22] Itano W M, Bergquist J C, Bollinger J J, Gilligan J M, Heinzen D J, Moore F L, Raizen M G and Wineland D J 1993 *Phys. Rev. A* **47** 3554
[23] Berkeland D J, Miller J D, Bergquist J C, Itano W M and Wineland D J 1998 *J. Appl. Phys.* **83** 5025
[24] Shao H, Huang Y, Guan H, Qian Y and Gao K 2016 *Phys. Rev. A* **94** 042507
[25] Arora B, Safronova M S and Clark C W 2007 *Phys. Rev. A* **76** 064501
[26] Mitroy J, Safronova M S and Clark C W 2010 *J. Phys. B: At. Mol. Opt. Phys.* **43** 202001
[27] Safronova M S and Safronova U I 2011 *Phys. Rev. A* **83** 012503
[28] Barwood G P, Huang G, King S A, Klein H A and Gill P 2015 *J. Phys. B: At. Mol. Opt. Phys.* **48** 035401
[29] Huang Y, Liu Q, Cao J, Ou B, Liu P, Guan H, Huang X and Gao K 2011 *Phys. Rev. A* **84** 053841
[30] Dubé P, Madej A A, Bernard J E, Marmet L, Boulanger J S and Cundy S 2005 *Phys. Rev. Lett.* **95** 033001
[31] Shao H, Huang Y, Guan H, Li C, Shi T and Gao K 2017 *Phys. Rev. A* **95** 053415